Inorganic Chemistry

Article

pubs.acs.org/IC

Luminescence and Single-Molecule Magnet Behavior in Lanthanide Complexes Involving a Tetrathiafulvalene-Fused Dipyridophenazine Ligand

Fabrice Pointillart,*[,†] Julie Jung,[†] Romain Berraud-Pache,[†] Boris Le Guennic,*[,†] Vincent Dorcet,[†] Stéphane Golhen,[†] Olivier Cador,[†] Olivier Maury,[§] Yannick Guyot,[∥] Silvio Decurtins,[‡] Shi-Xia Liu,*[,‡] and Lahcène Ouahab[†]

[†]Institut des Sciences Chimiques de Rennes UMR 6226 CNRS-Université de Rennes 1, 35042 Rennes Cedex, France

[‡]Departement für Chemie und Biochemie, Universität Bern, Freiestrasse 3, CH-3012 Bern, Switzerland

[§]Laboratoire de Chimie, l'ENS-LYON-UMR 5182, 46 Allée d'Italie, 69364 Lyon Cedex 07, France

[∥]Institut Lumière Matière, UMR 5306 CNRS-Université de Lyon 1, 10 rue Ada Byron, 69622 Villeurbanne Cedex, France

Supporting Information

ABSTRACT: The reaction between the TTF-fused dipyrido[3,2-*a*:2′,3′-*c*]-phenazine (dppz) ligand (**L**) and 1 equiv of $Ln(hfac)_3{\cdot}2H_2O$ ($hfac^-$ = 1,1,1,5,5,5-hexafluoroacetyacetonate) or 1 equiv of $Ln(tta)_3{\cdot}2H_2O$ (tta^- = 2-thenoyltrifluoroacetonate) (Ln^{III} = Dy^{III} or Yb^{III}) metallic precursors leads to four mononuclear complexes of formula $[Ln(hfac)_3(\mathbf{L})]{\cdot}C_6H_{14}$ (Ln^{III} = Dy^{III} (**1**), Yb^{III} (**2**)) and $[Ln(tta)_3(\mathbf{L})]{\cdot}C_6H_{14}$ (Ln^{III} = Dy^{III} (**3**), Yb^{III} (**4**)), respectively. Their X-ray structures reveal that the Ln^{III} ion is coordinated to the bischelating nitrogenated coordination site and adopts a D_{4d} coordination environment. The dynamic magnetic measurements show a slow relaxation of the Dy^{III} magnetization for **1** and **3** with parameters highlighting a slower relaxation for **3** than for **1** (τ_0 = 4.14(±1.36) × 10^{-6} and 1.32(±0.07) × 10^{-6} s with Δ = 39(±3) and 63.7(±0.7) K). This behavior as well as the orientation of the associated magnetic anisotropy axes have been rationalized on the basis of both crystal field splitting parameters and ab initio SA-CASSCF/RASSI-SO calculations. Irradiation of the lowest-energy HOMO → LUMO ILCT absorption band induces a $^2F_{5/2} \rightarrow {}^2F_{7/2}$ Yb-centered emission for **2** and **4**. For these Yb^{III} compounds, Stevens operators method has been used to fit the thermal variation of the magnetic susceptibilities, and the resulting M_J splittings have been correlated with the emission lines.

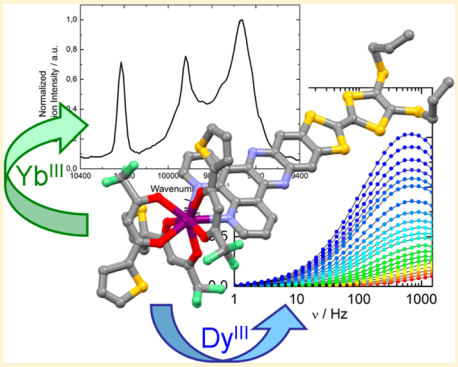

INTRODUCTION

In the molecular magnetism field of research, lanthanide ions take a preponderant place due to their intrinsic magnetic and luminescence properties. Indeed, such elements are well-known candidates to elaborate single-molecule magnets (SMM) because of their strong single-ion anisotropy and large magnetic moment.[1] SMM behavior can be observed in single lanthanide complexes using a plethora of organic ligands such as the 1,4,7,10-tetraazacyclododecane-*N*,*N*′,*N*″,*N*‴-tetraacetic acid,[2] organometallic sandwich ligand,[3] or phthalocyaninate.[4] In all these systems, coordinated ligands drive obtaining the desired axial magnetic anisotropy (Ising anisotropy) thanks to an adequate charge distribution around the lanthanide center.[5]

In addition, lanthanide ions are widely studied for their specific luminescence properties with emission line-like spectra ranging from visible to near-infrared (NIR) and luminescence lifetimes from microseconds to milliseconds.[6] These emission properties are exploited usually for applications in bioimaging,[7] optical telecommunication devices,[8] or material science (e.g., OLED).[9] In the context of molecular magnetism, the luminescence of lanthanide is correlated directly to the magnetic properties since it can be described as a picture of the energy splitting of the ground-state multiplet under crystal field interaction, which is also responsible for the magnetic properties. In this particular case, the organic ligand which permits stabilizing the Ising anisotropy is also used as an organic chromophore to sensitize the lanthanide luminescence.[2b,c,10]

The main part of our research is focused on the tetrathiafulvalene (TTF)/lanthanide couple. Even if TTF has been implied mainly in molecular conductors[11] due its redox activity, it is also a remarkable (i) organic chromophore to efficiently sensitize visible and NIR luminescence of lanthanides[12] and (ii) structural agent to build redox-active SMM.[13] Herein, we focus on the specific TTF-fused dipyrido[3,2-*a*:2′,3′-*c*]phenazine (dppz) ligand (**L**) which has been synthesized previously by some of us (Scheme 1).[14]

Received: February 23, 2015
Published: May 12, 2015

DOI: 10.1021/acs.inorgchem.5b00441
Inorg. Chem. 2015, 54, 5384−5397

Scheme 1. Chemical Structure of L

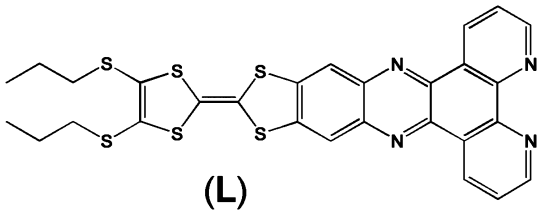

(L)

This electron donor−acceptor (D−A) ligand displays (i) promising electronic interactions such as a strong intramolecular ligand charge transfer (ILCT) band in the visible spectral region, (ii) redox activity, and (iii) a dipyridyl moiety suitable for coordination of metal precursors[15] for obtaining SMM behavior. It is also useful for sensitization of the lanthanide luminescence by the antenna effect.[9,14e,15]

Herein, we present the coordination reactions of the Ln(β-diketonate)$_3$·2H$_2$O (Ln^{III} = Dy^{III} and Yb^{III}, β-diketonate = 1,1,1,5,5,5-hexafluoroacetylacetonate ($hfac^-$) and 2-thenoyltrifluoroacetonate (tta^-)) with the ligand (**L**) and the X-ray structures of [Ln(hfac)$_3$(**L**)]·C$_6$H$_{14}$ and [Ln(tta)$_3$(**L**)]·C$_6$H$_{14}$. In addition, static and dynamic magnetic properties are experimentally and theoretically (using both Stevens operators technique and ab initio SA-CASSCF/RASSI-SO calculations) investigated. The photophysical properties have been determined and rationalized by time-dependent density functional theory (TD-DFT). Finally, for the Yb^{III} derivatives, the correlation between magnetic and luminescence properties is discussed.

EXPERIMENTAL SECTION

Synthesis, General Procedures, and Materials. The precursors Ln(hfac)$_3$·2H$_2$O (Ln^{III} = Dy and Yb; $hfac^-$ = 1,1,1,5,5,5-hexafluoroacetylacetonate anion), Ln(tta)$_3$·2H$_2$O (Ln^{III} = Dy and Yb; tta^- = 2-thenoyltrifluoroacetonate anion) and the ligand **L** were synthesized following previously reported methods.[14,16] All other reagents were commercially available and used without further purification.

Synthesis of Complexes 1−4. *[Ln(hfac)$_3$(L)]·C$_6$H$_{14}$ (Ln = Dy^{III} (1) and Ln = Yb^{III} (2)).* A 0.02 mmol amount of Ln(hfac)$_3$·2H$_2$O was dissolved in 5 mL of CH_2Cl_2 and then added to a solution of 5 mL of CH_2Cl_2 containing 12.1 mg of **L** (0.02 mmol). After 15 min of stirring, 10 mL of *n*-hexane was added at room temperature. Slow evaporation of the mixture gives dark blue single crystals which are suitable for X-ray studies. Yield: 23 (77%) and 25 mg (83%), respectively, for compounds **1** and **2**. Anal. Calcd for $C_{49}H_{39}DyF_{18}N_4O_6S_6$: C, 39.82; H, 2.64; N, 3.79. Found: C, 39.15; H, 2.46; N, 3.81. Anal. Calcd for $C_{49}H_{39}YbF_{18}N_4O_6S_6$: C, 39.54; H, 2.62; N, 3.77. Found: C, 39.29; H, 2.54; N, 3.79.

[Ln(tta)$_3$(L)]·C$_6$H$_{14}$ (Ln = Dy^{III} (3) and Ln = Yb^{III} (4)). A 0.02 mmol amount of Ln(tta)$_3$·2H$_2$O was dissolved in 5 mL of CH_2Cl_2 and then added to a solution of 5 mL of CH_2Cl_2 containing 12.1 mg of **L** (0.02 mmol). After 15 min of stirring, 10 mL of *n*-hexane was added at room temperature. Slow evaporation of the mixture gives dark blue single crystals which are suitable for X-ray studies. Yield: 26 (84%) and 27 mg (87%), respectively, for compounds **1** and **2**. Anal. Calcd for $C_{58}H_{48}DyF_9N_4O_6S_9$: C, 45.82; H, 3.16; N, 3.69. Found: C, 45.59; H, 3.04; N, 3.77. Anal. Calcd for $C_{58}H_{48}YbF_9N_4O_6S_9$: C, 45.51; H, 3.14; N, 3.66. Found: C, 45.25; H, 3.06; N, 3.71.

Crystallography. Single crystals of **1**−**4** were mounted on a APEXII Bruker-AXS diffractometer for data collection (Mo Kα radiation source, λ = 0.71073 Å). The structures were solved by direct methods using the SIR-97 program and refined with a full matrix least-squares method on F^2 using the SHELXL-97 program[17] for **1** and **2**, while only a cell determination was performed for **3** and **4**. Crystallographic data are summarized in Table 1. Complete crystal structure results as a CIF file including bond lengths, angles, and atomic coordinates are deposited as Supporting Information.

Physical Measurements. Elemental analyses of the compounds were performed at the Centre Régional de Mesures Physiques de l'Ouest, Rennes. Absorption spectra were recorded on a Varian Cary 5000 UV-visible-NIR spectrometer equipped with an integration sphere. The luminescence spectra were measured using a Horiba-Jobin Yvon Fluorolog-3 spectrofluorimeter, equipped with a three-slit double-grating excitation and emission monochromator with dispersions of 2.1 nm/mm (1200 grooves/mm). The steady-state luminescence was excited by unpolarized light from a 450 W xenon CW lamp and detected at an angle of 90° for diluted solution measurements or at 22.5° for solid-state measurement (front face detection) by a red-sensitive Hamamatsu R928 photomultiplier tube. Spectra were reference corrected for both the excitation source light

Table 1. X-ray Crystallographic Data for 1−4

	[Dy(hfac)$_3$(**L**)]·C$_6$H$_{14}$ (**1**)	[Yb(hfac)$_3$(**L**)]·C$_6$H$_{14}$ (**2**)	[Dy(tta)$_3$(**L**)]·C$_6$H$_{14}$ (**3**)	[Yb(tta)$_3$(**L**)]·C$_6$H$_{14}$ (**4**)
formula	$C_{49}H_{39}DyF_{18}N_4O_6S_6$	$C_{49}H_{39}YbF_{18}N_4O_6S_6$	$C_{58}H_{48}DyF_9N_4O_6S_9$	$C_{58}H_{48}YbF_9N_4O_6S_9$
M (g mol^{-1})	1476.7	1487.2	1519.0	1529.5
cryst syst	monoclinic	monoclinic	orthorhombic	orthorhombic
space group	*C*2/*c* (No.15)		*Pbna* (No. 60)	
cell params	*a* = 22.0242(19) Å	*a* = 21.8981(164) Å	*a* = 19.4111(11) Å	*a* = 19.3855(323) Å
	b = 32.6538(32) Å	*b* = 32.7491(223) Å	*b* = 20.99910(11) Å	*b* = 20.9534(304) Å
	c = 21.5688(21) Å	*c* = 21.4049(160) Å	*c* = 34.2648(16) Å	*c* = 34.1989(567) Å
	β = 128.9194(28)°	*β* = 128.4327(160)°		
volume (Å^3)	12 068.6(30)	12 024.5(246)	13 961.5(13)	13 891.3(624)
Z	8	8	8	8
T (K)	150 (2)	150 (2)	150(2)	150(2)
2*θ* range (deg)	6.04 ≤ 2*θ* ≤ 54.96		2.38≤ 2*θ* ≤ 54.92	
ρ_{calcd} (g·cm^{-3})	1.625		1.445	
μ (mm^{-1})	1.550		1.411	
no. of reflns	52 781		66 074	
no. of independent reflns	13 794		158 97	
R_{int}	0.1820		0.0620	
$F_o^2 > 2\sigma(F_o)^2$	5296		6497	
no. of variables	727		648	
R_1, wR_2	0.0776, 0.1416		0.0962, 0.2606	

DOI: 10.1021/acs.inorgchem.5b00441
Inorg. Chem. 2015, 54, 5384−5397

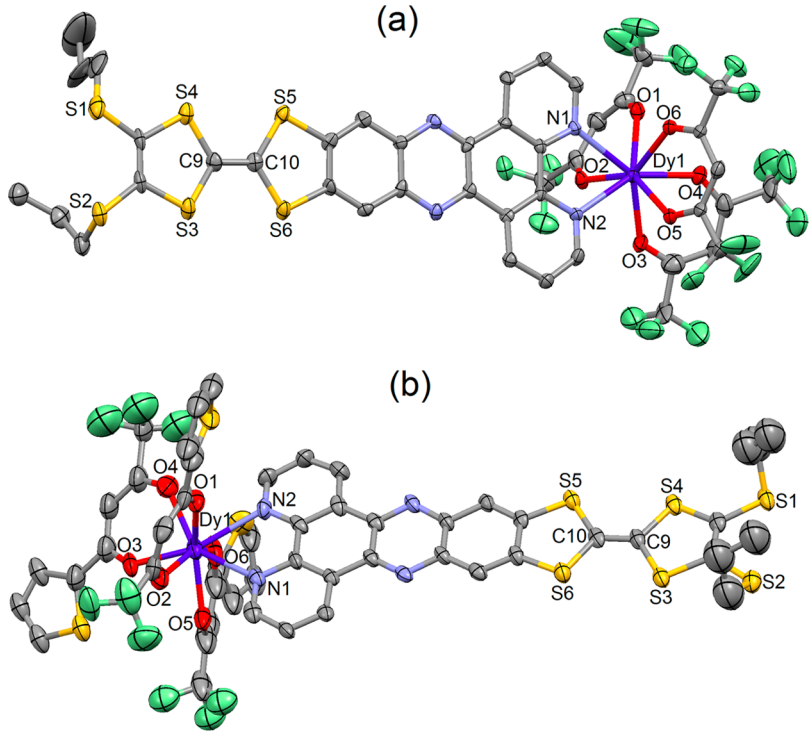

Figure 1. ORTEP view of the mononuclear complexes $[Dy(hfac)_3(\mathbf{L})]\cdot C_6H_{14}$ (**1**) (a) and $[Dy(tta)_3(\mathbf{L})]\cdot C_6H_{14}$ (**3**) (b). Thermal ellipsoids are drawn at 30% probability. Hydrogen atoms and *n*-hexane molecules are omitted for clarity.

intensity variation (lamp and grating) and the emission spectral response (detector and grating). Near-infrared spectra were recorded at an angle of 45° using a liquid-nitrogen-cooled, solid indium/gallium/arsenic detector (850−1600 nm). The luminescence decay of ytterbium complexes was determined using a homemade set up. The excitation of the Yb^{III} luminescence decays was performed with an optical parametric oscillator from EKSPLA NT342, pumped with a pulsed frequency tripled YAG:Nd laser. The pulse duration was 6 ns at 10 Hz repetition rate. The detection was performed by a R1767 Hamamatsu photomultiplier through a Jobin−Yvon monochromator equipped with a 1 μm blazed grating. The signal was visualized and averaged with a Lecroy digital oscilloscope LT342. The dc magnetic susceptibility measurements were performed on solid polycrystalline sample with a Quantum Design MPMS-XL SQUID magnetometer between 2 and 300 K in an applied magnetic field of 0.2 T for temperatures of 2−20 K and 1 T for temperatures of 20−300 K. These measurements were all corrected for the diamagnetic contribution as calculated with Pascal's constants.

Computational Details. DFT geometry optimizations and TD-DFT excitation energy calculations of the ligand **L** and the Y^{III} derivatives of **2** and **4** were carried out with the Gaussian 09 (revision A.02) package[18] employing the PBE0 hybrid functional.[19] The "Stuttgart/Dresden" basis sets and effective core potentials were used to describe the yttrium atom,[20] whereas all other atoms were described with the SVP basis sets.[21] The first 50 monoelectronic excitations were calculated. In all steps, a modeling of bulk solvent effects (solvent = dichloromethane) was included through the polarizable continuum model (PCM)[22] using a linear-response nonequilibrium approach for the TD-DFT step.[23] Molecular orbitals were sketched using the Gabedit graphical interface.[24]

Wave function-based calculations were carried out first on the Dy^{III}-based complexes **1** and **3** extracted from X-ray crystal structures by using the SA-CASSCF/RASSI-SO approach, as implemented in the MOLCAS quantum chemistry package (version 8.0).[25] Moreover, in the case of **1**, the TTF ligand was simplified (with no further geometry optimization) as either a dipyrido[3,2-*a*:2′,3′-*c*]phenazine (**1dppz**), a dipyrido[3,2-*f*:2′,3′-*h*]quinoxaline (**1dpq**), or a 1,10-phenanthroline (**1phen**) ligand (Figure S7, Supporting Information) to analyze the role of the π system on the energy splitting of the ground multiplet and thus on the magnetic properties of the complexes. In this approach, the relativistic effects are treated in two steps on the basis of the Douglas−Kroll Hamiltonian. First, the scalar terms were included in the basis-set generation and used to determine the spin-free wave functions and energies in the complete active space self-consistent field (CASSCF) method.[26] Next, spin−orbit coupling was added within the restricted-active-space-state-interaction (RASSI-SO) method, which uses the spin-free wave functions as basis states.[27] The resulting wave functions and energies are used to compute the magnetic properties and *g* tensors of the lowest states from the energy spectrum by using the pseudospin $S = 1/2$ formalism in the SINGLE-ANISO routine.[28] Cholesky decomposition of the bielectronic integrals was employed to save disk space and speed-up the calculations.[29] The active space of the self-consistent field (CASSCF) method consisted of the nine 4f electrons of the Dy^{III} ion spanning the seven 4f orbitals, i.e., CAS(9,7)SCF. State-averaged CASSCF calculations were performed for all of the sextets (21 roots), all of the quadruplets (224 roots), and 300 out of the 490 doublets (due to software limitations) of the Dy^{III} ion. Twenty-one sextets, 128 quadruplets, and 107 doublets were mixed through spin−orbit coupling in RASSI-SO. All atoms were described by ANO-RCC basis sets.[30] The following contractions were used: [8s7p4d3f2g1h] for Dy; [4s3p2d] for the O and N directly coordinated to Dy; [4s3p] for the S atoms, [3s2p] for the C, N, and F atoms, and [2s] for the H atoms of the hfac/tta and **L** ligands. A similar procedure was then applied to the Yb^{III} complexes **2** and **4**. The active space consisted of 13 4f electrons in seven 4f orbitals, i.e., CAS(13,7)SCF. State-averaged CASSCF calculations were performed for the seven doublets of the Yb^{III} ion, all of which were included in the RASSI-SO calculation. The effects of dynamical correlation were treated by means of a CASPT2 treatment on top of the spin-free wave functions. Similar basis set contractions were used except for Yb, which was described at the [8s7p4d3f2g] level.

RESULTS AND DISCUSSION

Crystal Structures. *$[Ln(hfac)_3(L)]\cdot C_6H_{14}$ (Ln = Dy^{III} (1) and Ln = Yb^{III} (2)).* Compounds **1** and **2** are isostructural. The full

DOI: 10.1021/acs.inorgchem.5b00441
Inorg. Chem. 2015, 54, 5384−5397

data collection and structure refinement have been performed for **1**, whereby for **2** only the cell parameters have been determined to confirm its isomorphism (Table 1). Consequently, the structural description is given for **1**.

Compound **1** crystallizes in the *C*2/*c* (No. 15) monoclinic space group (Table 1). The asymmetric unit is composed of one $Dy(hfac)_3$ moiety, one **L** ligand, and one *n*-hexane interstitial solvent molecule (Figure 1a).

The Dy^{III} ion is surrounded by six oxygen atoms that belong to three $hfac^-$ ligands and two nitrogen atoms from the bis-chelating **L** ligand. As it is usually observed, the average Dy−O distance is shorter (2.331(7) Å) than the average Dy−N distance (2.518(7) Å) (Table 2) due to the oxophilic character

Table 2. Selected Bond Lengths (Angstroms) for Compounds 1 and 3

	1	3
Dy1−O1	2.336(7)	2.348(6)
Dy1−O2	2.357(6)	2.317(7)
Dy1−O3	2.341(7)	2.346(5)
Dy1−O4	2.296(7)	2.336(8)
Dy1−O5	2.322(7)	2.297(6)
Dy1−O6	2.332(6)	2.314(7)
Dy1−N1	2.539(7)	2.562(7)
Dy1−N2	2.497(7)	2.579(7)

of the lanthanide ion. The arrangement of the ligands leads to a distorted square antiprism (D_{4d} symmetry) coordination polyhedron around the Dy^{III} ion. This distortion is visualized by continuous shape measures performed with SHAPE 2.1 (Table 3).[31] The length of the central C=C bond of the TTF core is equal to 1.354(12) Å, which attests to the neutral form of **L**.

Table 3. SHAPE Analysis of the Coordination Polyhedron around the Lanthanide Ions in Complexes 1 and 3

	$CShM_{SAPR-8}$ (square antiprism) D_{4d}	$CShM_{BTPR-8}$ (biaugmented trigonal prism) C_{2v}	$CShM_{TDD-8}$ (triangular dodecahedron) D_{2d}
1	0.724	1.607	2.040
3	0.507	2.271	2.420

The crystal packing reveals the formation of "head-to-tail" dimers of **L** (donor−acceptor-type dimers) (Figure 2a) due to the close packing of the whole π system of the ligands. Two dimers interact through $\pi-\pi$ interactions of the dipyridophenazine acceptor moieties leading to the formation of pseudo zigzag chains (Figure 2b). No intermolecular S···S contacts are observed, and the shortest intermolecular Dy···Dy distance is equal to 9.813 Å.

*$[Ln(tta)_3(L)]\cdot C_6H_{14}$ (Ln = Dy^{III} (**3**) and Ln = Yb^{III} (**4**)).* The substitution of the $hfac^-$ ancillary anions by tta^- ones leads to similar mononuclear complexes, whereby both compounds **3** and **4** are isostructural. Full data collection and refinement of the structure have been performed only for **3**, while only the cell parameters have been determined in the case of **4** to confirm its isomorphism (Table 1). Consequently, the structural description is given for **3**. It crystallizes in the *Pbna* (No. 60) orthorhombic space group (Table 1). The asymmetric unit is composed of one $Dy(tta)_3$ moiety, one **L** ligand, and one *n*-hexane molecule of crystallization (Figure 1b). The Dy^{III} ion is surrounded by six oxygen atoms (average distance equal to 2.326(7) Å) that belong to three $hfac^-$ ligands and two nitrogen atoms (average distance equal to 2.571(7) Å) from the bis-chelating **L** ligand. The Dy−N distances in **1** are slightly shorter than in **3** due to the stronger electron-withdrawing effect of $hfac^-$ compared to tta^-. SHAPE analysis highlights for **3** a less distorted square antiprism as the coordination polyhedron of Dy^{III}, compared to **1**. The central C=C bond of the TTF core is equal to 1.325(10) Å, which attests to the neutral form of **L**. As for **1**, the crystal packing reveals the formation of dimers and zigzag chains (Figure S1, Supporting Information) with no short intermolecular S···S contacts; the shortest intermolecular Dy···Dy distance is significantly longer (11.371 Å) compared to **1**.

Electrochemical Properties. The redox properties of **L** and the related complexes **1**−**4** are investigated by cyclic voltammetry (Figures 3 and S2, Supporting Information), and the values of the oxidation potentials are listed in Table 4.

The cyclic voltammogram of **L** shows two one-electron oxidations at 0.69 and 1.06 V corresponding to the formation of a radical cation and a dication TTF moiety, respectively (Figure 3). Previous work on the free ligand demonstrated the reversibility of the first oxidation wave but not for the second one, highlighting the instability of the dication.[14] The measured oxidation potentials are higher (from +0.1 to +0.2 V) than those found for the functionalized TTF donor[32] due to the strong electron-withdrawing effect of the dipyridophenazine acceptor. Upon coordination of the lanthanide ions, surprisingly, the electron-attracting $Ln(hfac)_3$ and $Ln(tta)_3$ fragments have no significant effect on the oxidation potentials (Table 4). In addition, **L** also revealed a reversible one-electron reduction process which was attributed to the formation of the phenazine radical anion.[14] In the actual lanthanide complexes this reduction wave is only fairly observed around a potential of −1.23 V (vs SCE) (Figure S2, Supporting Information). This value may correspond to the one for the free ligand (−1.17 V vs Ag/AgCl). The reversibility of the first oxidation potential is conserved, and the electrochemical properties demonstrate the redox activity of **L** in the complexes.

Magnetic Properties. *Static Measurements.* The thermal variations of the $\chi_M T$ products for **1**−**4** are given in Figure 4. All $\chi_M T$ products show a monotonic decrease in the 300−2 K temperature range taking values of 14.12 and 11.08 cm^3 K mol^{-1} for complex **1**, 2.41 and 1.06 cm^3 K mol^{-1} for complex **2**, 13.92 and 11.67 cm^3 K mol^{-1} for complex **3**, and 2.37 and 1.09 cm^3 K mol^{-1} for complex **4** at room and low temperatures, respectively. The experimental room-temperature values of $\chi_M T$ are in agreement with the theoretical values of 14.17 and 2.57 cm^3 K mol^{-1} expected for magnetically isolated Dy^{III} and Yb^{III} ions.[33] The first magnetization curves measured at 2 K show classical behavior in the field range 0−5 T for magnetically isolated lanthanides such as those involved in complexes **1**−**4** (Figure S3, Supporting Information). The magnetic properties of compounds **2** and **4** were analyzed in the framework of the Stevens operators technique, whereas those of compounds **1** and **3** were discussed based on the results of ab initio calculations (see next section). In the equivalent operators model the crystal field splitting is described by polynomials of the total angular momentum (J^2, J_z, J_+, and J_-)

DOI: 10.1021/acs.inorgchem.5b00441
Inorg. Chem. 2015, 54, 5384−5397

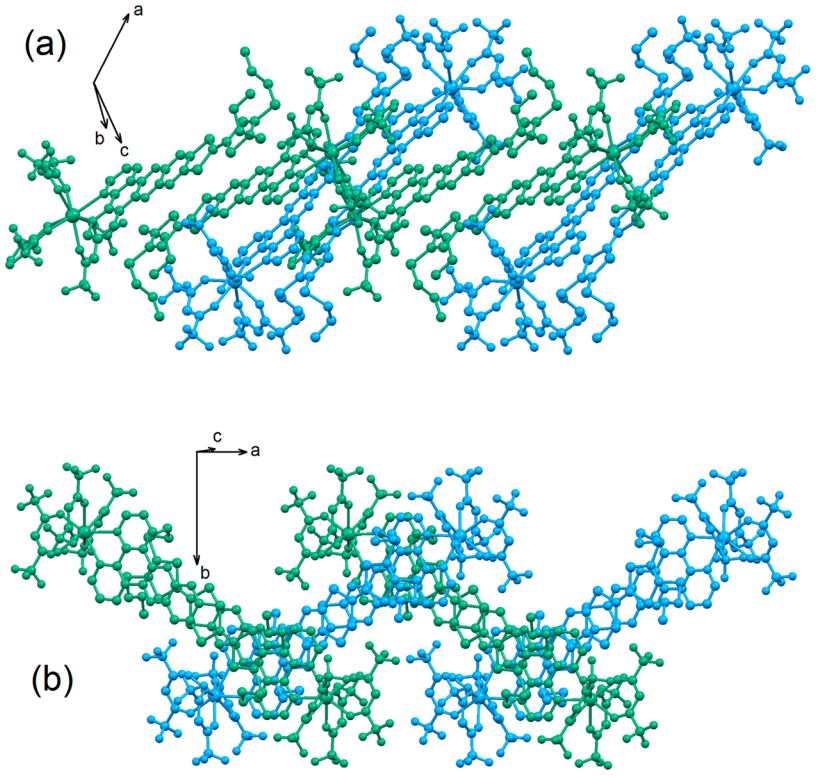

Figure 2. Crystal packing of **1** highlighting the formation of dimers of **L** (a) and a pseudo zigzag chain through the packing of the highlighted dimers (b).

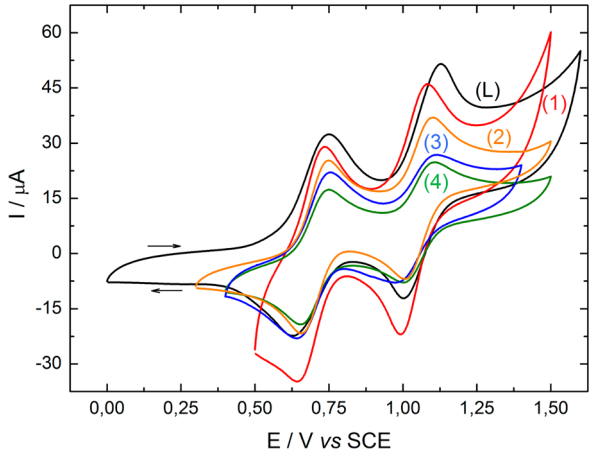

Figure 3. Cyclic voltammetry of ligand **L** and compounds **1**–**4** in CH_2Cl_2 at a scan rate of 100 $mV{\cdot}s^{-1}$ with $[N(C_4H_9)_4]PF_6$ as supporting electrolyte (0.1 M). Potentials were measured vs a saturated calomel electrode (SCE), glassy carbon working electrode, and Pt wire counter electrode.

Table 4. Oxidation Potentials (V vs SCE, nBu_4NPF_6, 0.1 M in CH_2Cl_2 at 100 $mV{\cdot}s^{-1}$) of the Ligand L and Complexes 1–4

	$E^1_{1/2}$	$E^2_{1/2}$
L	0.69	1.06
1	0.69	1.04
2	0.70	1.05
3	0.70	1.05
4	0.70	1.05

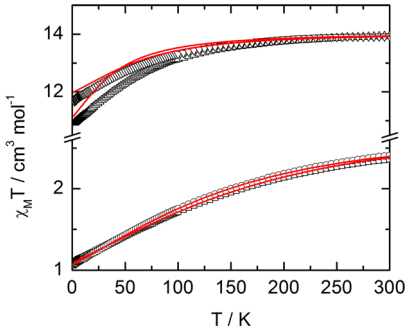

Figure 4. Thermal variation of $\chi_M T$ for **1** (up triangles), **2** (circles), **3** (down triangles), and **4** (squares). Red lines correspond to the best-fitted curves with Stevens operators technique for **2** and **4** and to the curves simulated from ab initio calculations for **1** and **3**.

$$\hat{H} = B_2^0\widehat{\mathbf{O}}_2^0 + B_2^2\widehat{\mathbf{O}}_2^2 + B_4^0\widehat{\mathbf{O}}_4^0 + B_4^2\widehat{\mathbf{O}}_4^2 + B_4^4\widehat{\mathbf{O}}_4^4 + B_6^0\widehat{\mathbf{O}}_6^0 + B_6^2\widehat{\mathbf{O}}_6^2 + B_6^4\widehat{\mathbf{O}}_6^4 + B_6^6\widehat{\mathbf{O}}_6^6$$

where the $\widehat{\mathbf{O}}_k^q$'s are the operators equivalents and the B_k^q's are connected to the crystal field parameters.[34] The perturbation due to the application of an external magnetic field can easily be estimated, and the magnetization can be calculated. In a D_{4h} environment, only the B_k^0's are nonzero.[35] In this frame, the best fits are obtained with $B_2^0 = 1.1906(5)$ cm^{-1}, $B_4^0 = 0.405(6)$ cm^{-1}, and $B_6^0 = 1.03(5) \times 10^{-3}$ cm^{-1} for compound **2** and $B_2^0 = 1.190(4)$ cm^{-1}, $B_4^0 = 0.474(7)$ cm^{-1}, and $B_6^0 = 1.04(4) \times 10^{-3}$ cm^{-1} for compound **4**, all in good agreement with experiments (Figure 4). In such a high symmetry, M_J remains a good

DOI: 10.1021/acs.inorgchem.5b00441
Inorg. Chem. 2015, 54, 5384–5397

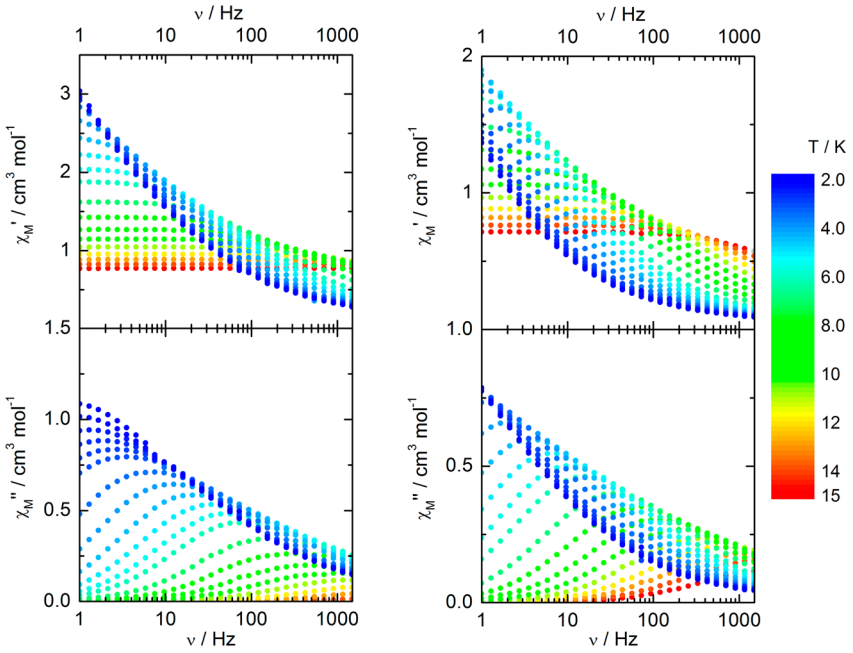

Figure 5. Frequency dependences of the in-phase and out-of-phase components of the ac susceptibility measured in the 2−15 K temperature range for **1** (left) and **3** (right) at 1 kOe external dc field.

quantum number and the ground states correspond for both compounds to the $M_J = \pm 5/2$ component of the ground-state multiplet. The calculated M vs H curves at 2 K reproduce almost perfectly the experiments (Figure S3, Supporting Information), which certifies that the ground states are properly described. The total splitting of the multiplet ground-state $^2F_{7/2}$ is calculated at an energy equal to 515 and 681 cm^{-1} for **2** and **4**, respectively. The first excited state ($M_J = \pm 3/2$) is localized at 247 (for **2**) and 271 cm^{-1} (for **4**) above the ground state. The second ($M_J = \pm 1/2$) and third excited states ($M_J = \pm 7/2$) are, respectively, localized at 513 and 515 cm^{-1} (for **2**) and 584 and 681 cm^{-1} (for **4**).

Dynamic Measurements. No out-of-phase signals (χ_M'') of the ac susceptibility are detected in zero field for **2** and **4**. On the contrary, **1** and **3** display clear thermally activated frequency-dependent out-of-phase signals (Figure S5, Supporting Information). At low temperature a fast thermally-independent process maintains the maximum of χ_M'' outside the window of accessible frequencies for **1** and just at the limit for **3**. The relaxation times of such thermally-independent processes can be estimated to be 5×10^{-5} s for **1** and 2.6×10^{-4} s for **3** from a fitting procedure with an extended Debye model (see Supporting Information). Nevertheless, it is clear that on cooling the maximum of the χ_M'' vs ν curves emerges at higher temperatures in **3** than in **1**. This is probably due to the fact that the energy barrier for **3** is higher. This behavior has already been observed in similar systems with identical N_2O_6 coordination polyhedra when the ancillary ligand $hfac^-$ is substituted by tta^-.[13e,36] The application of an external dc field dramatically shifts the maxima of χ_M'' to low frequencies (Figures 5, S6, and S7, Supporting Information). In both compounds, **1** and **3**, the optimum field, i.e., the field for which the maximum of the χ_M'' vs ν curves is at the lowest frequency, is estimated to be 1 kOe. Under these conditions the temperature variations of the relaxation times for **1** and **3** can be extracted from the ac susceptibility frequency scans treated with the extended Debye model (Tables S1 and S2, Supporting Information). The relaxation of the magnetic moment is slower for **3** than for **1**, independent of the temperature. In the high-temperature range, the temperature dependences of the relaxation time (Figure 6) can be reproduced with an Arrhenius law ($\tau = \tau_0 \exp(\Delta/T)$): $\tau_0 = 4.14(\pm 1.36) \times 10^{-6}$ and $1.32(\pm 0.07) \times 10^{-6}$ s with $\Delta = 39(\pm 3)$ and $63.7(\pm 0.7)$ K for **1** and **3**, respectively.

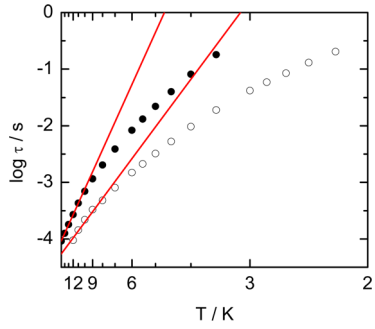

Figure 6. Temperature dependences of the relaxation times (τ) at 1 kOe for **1** (empty circles) and **3** (full circles) with the best fitted curves with an Arrhenius law (red lines).

Ab Initio Calculations. SA-CASSCF/RASSI-SO calculations were performed first on **1** and **3** to rationalize the observed magnetic properties (see Computational Details). First, the effect of the π system of the TTF ligand on the energy splitting of the ground-state multiplet $^6H_{15/2}$ and on the g tensor of the M_J ground state was investigated for **1** considering three models, namely, **1ddpz**, **1dpq**, and **1phen** (Figure S8, Supporting Information), all obtained by simplification of the TTF ligand without subsequent geometry optimization. Energy spectra and g tensors for the eight Kramer's doublets of the ground $^6H_{15/2}$ multiplet of the Dy^{III} ion are given in Figure S8 and Table S3, Supporting Information. As one may expect, the modulation of the electronic effect of the ligand due to increased π conjugation has no significant influence on the

DOI: 10.1021/acs.inorgchem.5b00441
Inorg. Chem. 2015, 54, 5384−5397

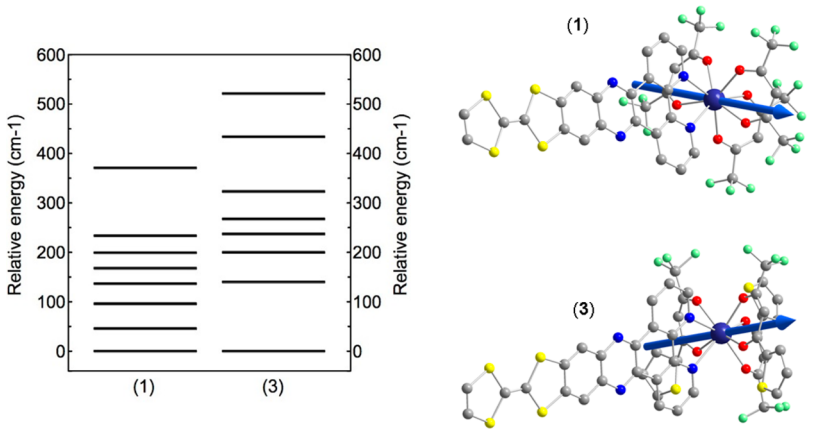

Figure 7. Energy splitting of the $^6H_{15/2}$ multiplet (left) and anisotropy axis (right) for **1** and **3**.

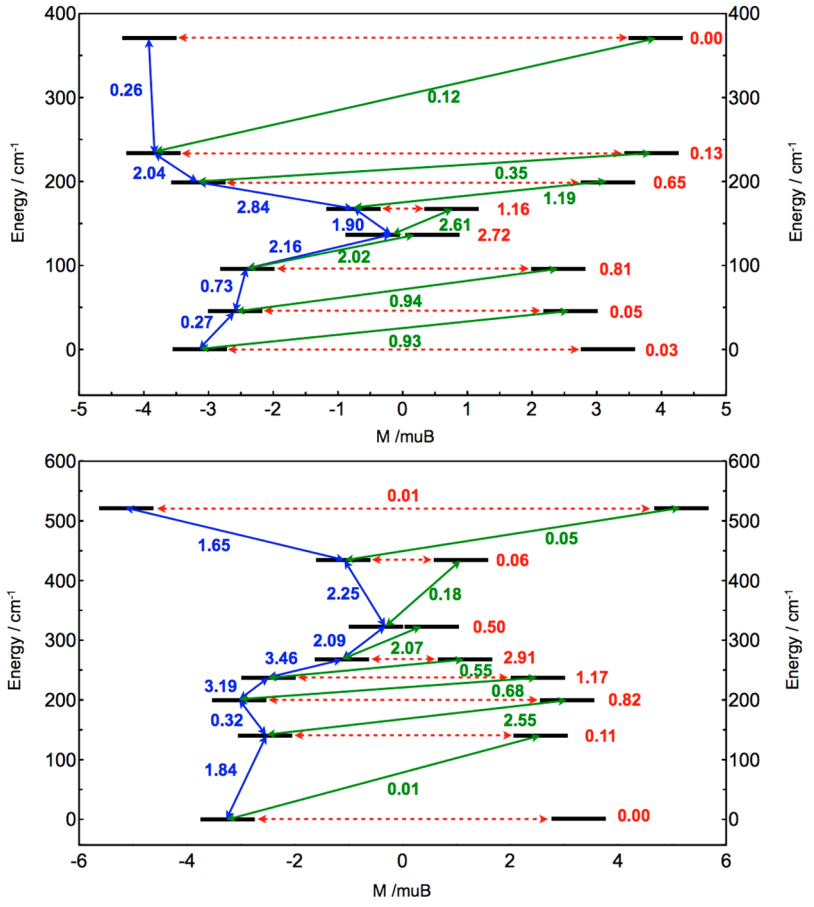

Figure 8. Computed magnetization blocking barriers in complexes **1** (top) and **3** (bottom). Numbers provided on each arrow are the mean absolute values for the corresponding matrix elements of the magnetic transition dipole moment.

energy spectra and g tensor. The energy splitting of the $^6H_{15/2}$ multiplet is almost identical for the four models, leading to a similar thermal dependence of the $\chi_M T$ products. The orientation of the easy magnetization axis is also not affected. These results are in potential contradiction with recently published experimental results[37] that proposed that electronic reorganizations related to the extension of the π system are responsible for increasing the anisotropy barrier for similar Dy^{III} complexes as those studied here. However, the experimental barrier should evidently not be only considered as the only energy difference between the ground and the first excited states since various mechanisms are potentially involved. Subsequent studies are in progress to confirm this statement.

Let us now concentrate on the comparison between **1** and **3**. Both $\chi_M T$ vs T and M vs H curves are fairly well reproduced for **3** (Figures 4 and S3, Supporting Information). The agreement is not as good for **1**, probably due to a slight underestimation of the gap between the ground and the first excited states (Figure 7). It is clear however that this gap is smaller in **1** than in **3**.

Moreover, calculations confirm the axial character of the magnetic anisotropy tensor of the ground Kramer's doublet with large g_z values of 18.89 for **1** and 19.58 for **3** and small g_x

DOI: 10.1021/acs.inorgchem.5b00441
Inorg. Chem. 2015, 54, 5384−5397

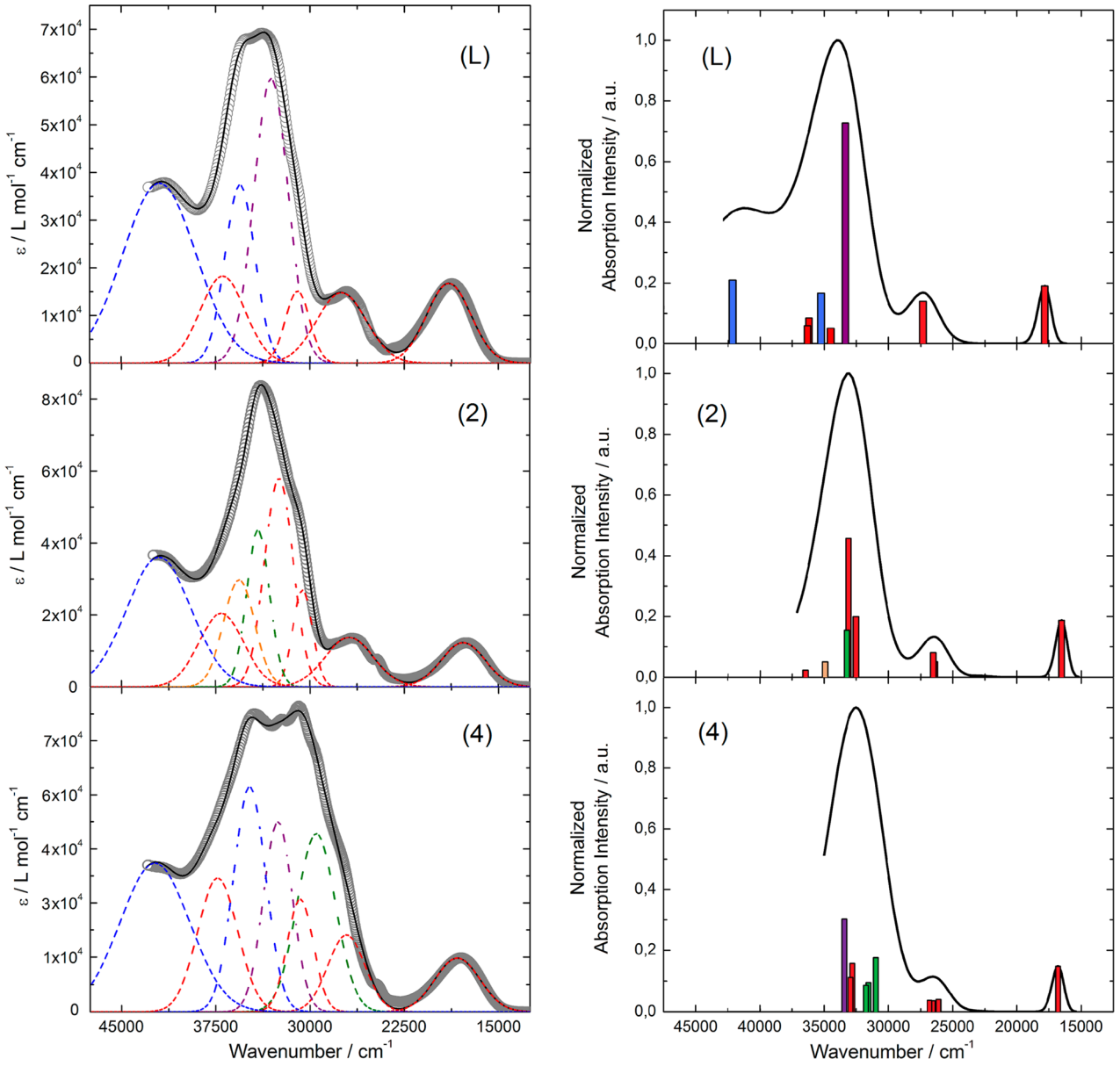

Figure 9. (Left) Experimental UV−vis absorption spectra in CH_2Cl_2 solution of **L**, **2**, and **4** ($C = 4 \times 10^{-5}$ mol L^{-1}) (open gray circles). Respective Gaussian decompositions (dashed lines) and best fit (full black line) (R^2 = 0.9987 for **L**, R^2 = 0.9989 for **2**, and R^2 = 0.9985 for **4**). (Right) Theoretical absorption spectra of **L** and the Y^{III} analogue of **2** and **4** (black line). Sticks represent the main contributions of the absorption spectra.

and g_y values. As commonly found when comparing complexes bearing either tta^- or $hfac^-$ ligands,[13e] it clearly appears that the g_z value for **3** is closer to the expected $g_z = 20$ for a pure $M_J = \pm 15/2$ ground state than for **1**. Magnetic relaxation pathways can be interpreted on the basis of magnetic transition moments (Figure 8). Whereas for **3** magnetic relaxation may involve the first excited state, a more direct relaxation pathway is expected for **1**. All results confirm, at least qualitatively, the trend observed in the dynamic magnetic properties of the compounds, i.e., the relaxation of the magnetic moment is 2.5 times slower for **3** than for **1**. Changing $hfac^-$ by tta^- anions implies (i) a more regular D_{4d} symmetry of the Dy^{III} surrounding and (ii) an electronic redistribution of the charge on the first neighboring atoms. The calculated ground-state easy axis (Figure 7) is oriented perpendicular to the plane formed by the TTF-based ligand, as expected for an oblate ion. The negative charges on the oxygen atoms are substantially higher than on the nitrogen ones, inducing the electrostatic anisotropy that governs the orientation of the ground-state magnetic easy axis.

A similar ab initio protocol was also applied to both Yb^{III} compounds **2** and **4**. However, as usual for Yb^{III} complexes,[38] dynamical correlation effects had to be taken into account by means of CASPT2 calculations (see Computational Details). As seen in Figure S4, Supporting Information, good agreement is obtained only for **2** at low temperature, whereas this is far from the case for **4**. This difficulty in reproducing the experimental magnetic data of Yb^{III} complexes using CASPT2 calculations is already known, as reflected by the limited number of works devoted to ab initio simulations of the magnetic properties of Yb^{III} complexes,[2c,38,39] compared to the numerous examples already existing for Dy^{III} complexes. An explanation can be found in the difficulties to properly describe the more complex electronic structure of Yb^{III} complexes with respect to Dy^{III} due

DOI: 10.1021/acs.inorgchem.5b00441
Inorg. Chem. 2015, 54, 5384−5397

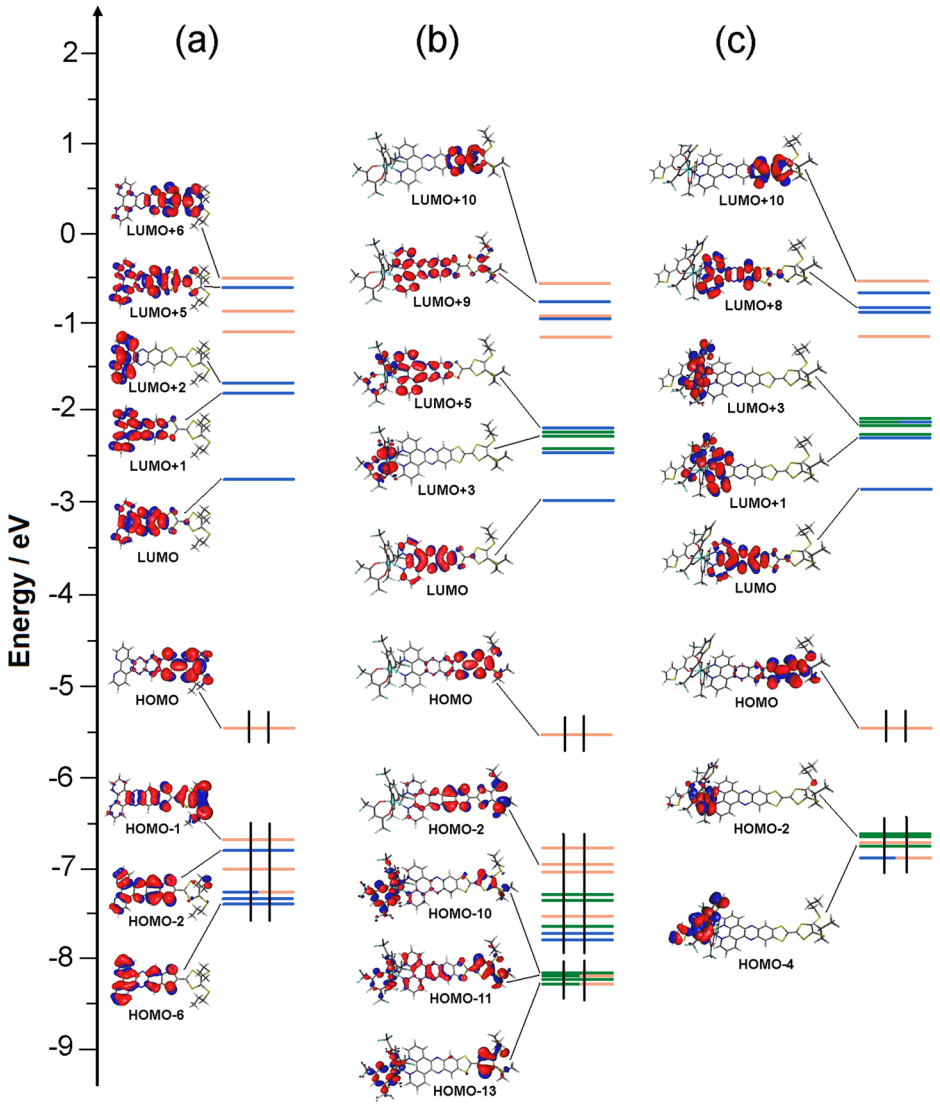

Figure 10. MO diagram of **L** (a) and the Y^{III} analogue of **2** (b) and **4** (c). Energy levels of the centered TTF donor, dipyridophenazine acceptor, and hfac/tta$^-$ anions are shown in orange, blue, and green, respectively.

to (nonexhaustively) (i) the number of 4f electrons, (ii) the importance of dynamical correlation, and (iii) the propensity of having Yb^{III}/Yb^{II} mixing in the ground-state wave function.

Photophysical Properties. *Absorption Properties.* The UV−vis absorption properties of **L**, **2**, and **4** have been studied in a CH_2Cl_2 solution (Figure 9). Rationalization based on TD-DFT calculations was performed on the Y^{III} analogues following a computational strategy already used successfully on other TTF-based systems.[40] The molecular orbital diagram and UV−vis absorption spectra were calculated for **L** and the Y^{III} analogue of **2** and **4** (Figures 9 and 10, Table 6).

The experimental absorption spectrum of **L** was decomposed into seven bands. The calculated UV−vis absorption spectrum for **L** was already studied,[14] but calculations were repeated in the present work in order to perfectly compare them with the respective coordination complexes. The calculated spectrum reproduces well the experimental curve (Figure 9). The three lowest energy bands were attributed to TTF to dipyridophenazine charge transfers (ILCT) (red Gaussian decompositions) (Figure 9, Table 6). The calculated values of the absorption maxima are very close to the experimental ones (Table 6). The ILCTs are identified as $\pi-\pi^*$ HOMO → LUMO (17 844 cm^{-1}), HOMO−1 → LUMO (27 338 cm^{-1}), and HOMO → LUMO+5/+6 (34 504 cm^{-1}) (Figure 10). The intense absorption band experimentally centered at 33 100 cm^{-1} (purple decomposition) was calculated at 33 361 cm^{-1} and attributed to intraligand (IL) transitions (Table 6) with intra-acceptor (IA), intradonor (ID) and ILCT contributions. Finally, at the highest energy, the absorption bands were mainly attributed to IA transitions (blue decompositions).

The absorption spectra of **2** and **4** have been decomposed into eight bands (Figure 9 and Table 6). They show a new intense absorption band centered at 34 100 and 29 500 cm^{-1} that corresponds to $\pi-\pi^*$ intra-hfac$^-$ and $\pi-\pi^*$ intra-tta$^-$ excitations (green decompositions) for **2** and **4**, respectively.[14] As expected, the complexation induces a red shift of the lowest-energy ILCT transition due to the Lewis acid behavior of the Ln(β-diketonate)$_3$ moieties enforcing the electron-withdrawing character of the dipyridophenazine fragments.[41] Thus, the lowest energy absorption bands are red shifted by 1200 (for **2**) and 700 cm^{-1} (for **4**) in the coordination complexes compared to those in **L**. This trend is confirmed by TD-DFT calculations where energy stabilizations of 1300 and 1000 cm^{-1} for **2** and **4**, respectively, are found (Table 6). It is worth noticing that all

DOI: 10.1021/acs.inorgchem.5b00441
Inorg. Chem. 2015, 54, 5384−5397

Table 6. TD-DFT Excitation Energies and Main Compositions of the Low-Lying Electronic Transitions for L (a) and the Y^{III} Analogue of 2 (b) and 4 (c)[a]

E exp (cm^{-1})	E theo (cm^{-1})	osc.	type	assignment	transition
			a		
19 000	17 844	0.42	ILCT	$\pi_{TTF} \rightarrow \pi^*_{dppz}$	H → L (99%)
27 500	27 338	0.31	ILCT	$\pi_{TTF} \rightarrow \pi^*_{dppz}$	H-1 → L (80%)
31 000	34 504	0.11	ILCT	$\pi_{TTF} \rightarrow \pi^*_{dppz}$	H → L+5/+6 (56/33%)
33 100	33 361	1.61	IL	$\pi_{TTF} \rightarrow \pi^*_{TTF}$	H → L+6 (27%)
				$\pi_{TTF} \rightarrow \pi^*_{dppz}$	H → L+5 (31%)
				$\pi_{dppz} \rightarrow \pi^*_{dppz}$	H-2 → L+1 (30%)
35 600	35 252	0.37	IA	$\pi_{dppz} \rightarrow \pi^*_{dppz}$	H-2 → L+1 (29
36 900	36 195	0.19	ILCT	$\pi_{TTF} \rightarrow \pi^*_{dppz}$	H-1 → L+1/+2 (45/50%)
	36 315	0.13			
42 000	42 128	0.46	IA	$\pi_{dppz} \rightarrow \pi^*_{dppz}$	H-6 → L+2 (68%)
			b		
17 800	16 525	0.45	ILCT	$\pi_{TTF} \rightarrow \pi^*_{dppz}$	H → L (99%)
26 900	26 394	0.12	ILCT	$\pi_{TTF} \rightarrow \pi^*_{dppz}$	H-1/-2 → L (40/41%)
	26 510	0.19			H-1/-2 → L (52/32%)
30 600	32 533	0.48	ILCT	$\pi_{TTF} \rightarrow \pi^*_{dppz}$	H → L+7 (75%)
32 500	33 126	1.10	ID	$\pi_{TTF} \rightarrow \pi^*_{TTF}$	H → L+10 (19%)
			ILCT	$\pi_{TTF} \rightarrow \pi^*_{dppz}$	H → L+7/+9 (9/18%)
					H-6 → L (9%)
					H-2 → L+5 (13%)
34 100	33 242	0.37	Ihfac	$\pi_{hfac} \rightarrow \pi^*_{hfac}$	H-7/-9/-10 → L+3 (8/9/16%)
35 600	34 943	0.12	ID	$\pi_{TTF} \rightarrow \pi^*_{TTF}$	H-1 → L+6 (14%)
					H → L+10 (30%)
37 100	36 468	0.06	ILCT	$\pi_{TTF} \rightarrow \pi^*_{dppz}$	H-2/-3 → L+5 (15/31%)
42 000			IA	$\pi_{dppz} \rightarrow \pi^*_{dppz}$	
			c		
18 300	16 796	0.46	ILCT	$\pi_{TTF} \rightarrow \pi^*_{dppz}$	H → L (99%)
27 100	26 096	0.13	ILCT	$\pi_{tta} \rightarrow \pi^*_{dppz}$	H-1/-2 → L (53/38%)
	26 543	0.11		$\pi_{TTF} \rightarrow \pi^*_{dppz}$	H-3/-5 → L (54/34%)
	26 802	0.12			H-3/-5 → L (55/34%)
29 500	30 986	0.55	Itta	$\pi_{tta} \rightarrow \pi^*_{tta}$	H-4 → L+2 (67%)
	31 562	0.30			H-2 → L+3 (31%)
	31 745	0.27			H-1 → L+3/+4/+5 (16/13/25%)
30 800	32 804	0.49	ILCT	$\pi_{TTF} \rightarrow \pi^*_{dppz}$	H-5 → L+1 (18%)
	32 939	0.35			H-4 → L+1 (26%)
					H-1 → L+8 (32%)
32 600	33 443	0.95	IL	$\pi_{TTF} \rightarrow \pi^*_{dppz}$	H-1 → L+8 (29%)
				$\pi_{TTF} \rightarrow \pi^*_{TTF}$	H-1 → L+10 (30%)
34 800			IA	$\pi_{dppz} \rightarrow \pi^*_{dppz}$	
37 400			ILCT	$\pi_{TTF} \rightarrow \pi^*_{dppz}$	
42 300			IA	$\pi_{dppz} \rightarrow \pi^*_{dppz}$	

[a]In addition, the charge transfer and the pure intramolecular transitions are reported. ID, IA, and H and L represent the intramolecular TTF (donor) or dipyridophenazine (acceptor) and the HOMO and LUMO, respectively. ILCT stands for intraligand charge transfer.

the ILCT excitations are red shifted after complexation of the metal-containing fragment and the electron-attracting character of the $Ln(hfac)_3$ precursor is stronger than for $Ln(tta)_3$. This last effect enhances the CT character of the absorption band and leads to a change of the nature of the most intense excitation (centered at 32 500 cm^{-1}) in **2** from IL to ILCT.

Emission Properties. First, it is useful to remind that the free ligand **L** exhibits a weak fluorescence centered at 12 200 cm^{-1} under irradiation at 18 500 cm^{-1} in CH_2Cl_2 solution. The fluorescence lifetime was determined to be equal to 0.4 ns with a quantum yield of 1%.[14]

Emission properties of **2** (Figure 11a) and **4** (Figure 11b) were measured in the solid state at room temperature and 77 K. The values for **4** are given in brackets. Upon irradiation at 18 200 cm^{-1} [16 670 cm^{-1}] in the lowest-energy absorption band, which was attributed to the HOMO → LUMO ILCT transition, an emission centered at 10 200 cm^{-1} is detected that corresponds to the $^2F_{5/2} \rightarrow {}^2F_{7/2}$ transition. No significant residual ligand-centered emission is observed, indicating an efficient sensitization process. In solution, the same signal is observed, proof of the stability of the complexes in CH_2Cl_2, but bleached extremely rapidly under resonant irradiation. The solid-state luminescence spectra at low temperature are better resolved (Figure 11). At 77 K, the signal of **2** [**4**] allowed identifying several transitions at energies of 10 204, 9960, 9920, 9750, 9695, and 9630 cm^{-1} [10 214, 9920, 9745, 9660, and 9580 cm^{-1}]. The number of transition is higher than **4**, the expected number following the degeneracy of the $^2F_{7/2}$ ground state (Kramer's doublets), and additional transition may origin from vibronic or excited M_J states contributions.

DOI: 10.1021/acs.inorgchem.5b00441
Inorg. Chem. 2015, 54, 5384−5397

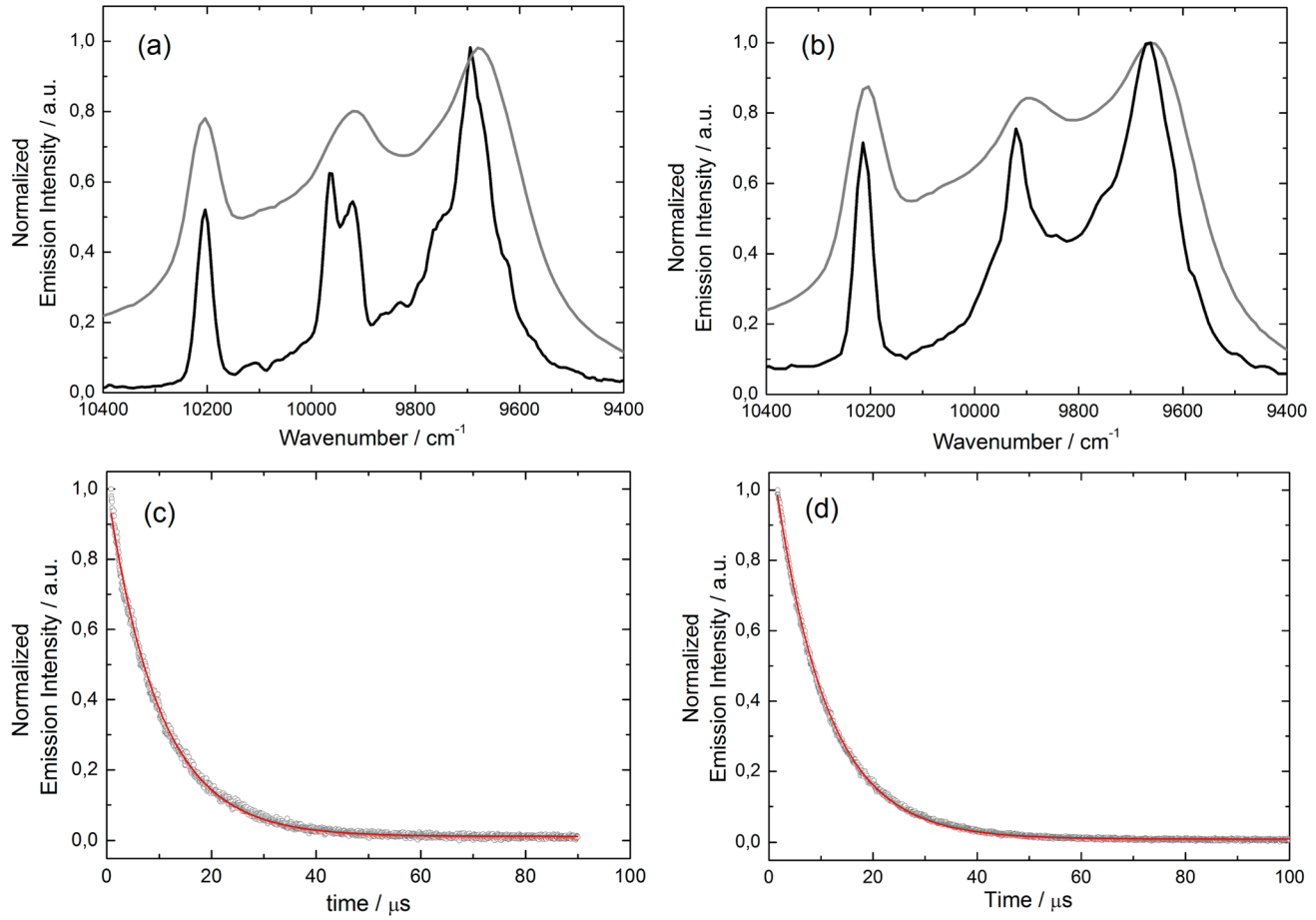

Figure 11. (a) Luminescence spectra of **2** in the NIR range for λ_{ex} = 18 200 cm^{-1} at room temperature (gray line) and 77 K (black line) in the solid state. (b) Luminescence spectra of **4** in the NIR range for λ_{ex} = 16 670 cm^{-1} at room temperature (gray line) and 77 K (black line) in the solid state. (c) Decay kinetic of $^2F_{5/2}$ recorded at 10 200 cm^{-1} in degassed CH_2Cl_2 at room temperature under 18 200 cm^{-1} excitation for **2** (c) and **4** (d). Red lines represent monoexponential fits.

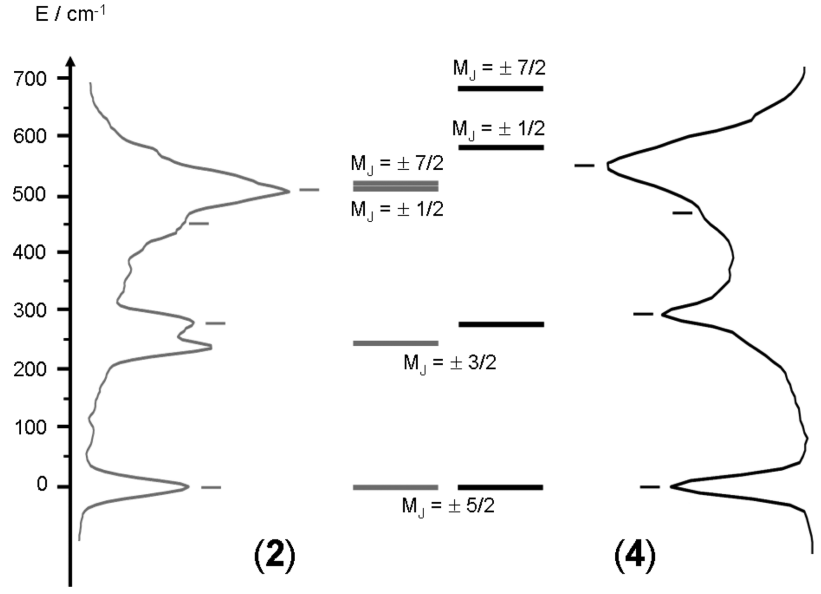

Figure 12. Solid-state 77 K emission spectra are represented with an appropriate shift of the energy scale. Diagram of energy levels for compounds **2** (full gray sticks) and **4** (full black sticks) calculated with the parameters given in the main text from the magnetic measurements. Labels correspond to the M_J values.

The total splitting is determined to be equal to 574 cm^{-1} [634 cm^{-1}]. The values of this splitting are 455 and 372 cm^{-1}, respectively, for an Yb^{III} ion in distorted and regular[35] D_3 symmetry, while a splitting value of 528 cm^{-1} is found for a

DOI: 10.1021/acs.inorgchem.5b00441
Inorg. Chem. 2015, 54, 5384−5397

Yb^{III} complex in low symmetry.[42] The value of 509 cm^{-1} seems to correspond to low symmetry that is in agreement with the presence of two nitrogen and six oxygen atoms in the first coordination sphere of Yb^{III}. SHAPE analysis gives the closest ideal symmetry without taking into account the nature of the coordinated atoms. Consequently, for the emission properties, a lower symmetry has to be taken into consideration, which results in a high-energy splitting and the clear appearance of more than four emission lines. At 77 K in frozen CH_2Cl_2 solution, the luminescence decay corresponds to a single-exponential function of the time. The $^2F_{5/2}$ state lifetime is measured equal to 9.9 and 9.45 μs for complexes **2** (Figure 11c) and **4** (Figure 11d), respectively. The emission spectrum at 77 K can be directly compared with the diagram obtained from magnetic measurements (Figure 12).[13h]

In the Russell−Saunders coupling scheme the emission spectrum is a picture of the ground-state multiplet splitting. The high-energy emission corresponds to transition to the ground state. The low-energy emission corresponds to a transition to the highest excited state of the $^2F_{7/2}$ multiplet. The calculated first excited level ($M_J = \pm 3/2$) (247 cm^{-1}) and [271 cm^{-1}] fits well the second emission line (+284 cm^{-1}) and [294 cm^{-1}]. The two highest-energy levels (513 and 515 cm^{-1}) [584 and 681 cm^{-1}] are higher in energy compared to the third (+454 cm^{-1}) [469 cm^{-1}] ($M_J = \pm 1/2$) and fourth (+509 cm^{-1}) [554 cm^{-1}] ($M_J = \pm 7/2$) emission lines. The most probable origin of this disagreement is due to the fact that the thermal population at room temperature of such high-energy M_J state is very low and therefore might not be localized precisely by thermal variation of the magnetic susceptibility.

CONCLUSIONS

Four mononuclear coordination complexes of formula [Ln(hfac)$_3$(**L**)]·C_6H_{14} (Ln = Dy^{III} (**1**) and Yb^{III} (**2**)) and [Ln(tta)$_3$(**L**)]·C_6H_{14} (Ln = Dy^{III} (**3**) and Yb^{III} (**4**)) have been synthesized. Their crystalline structures reveal that the lanthanide ions are coordinated to the bis-chelating nitrogenated dipyridophenazine acceptor and the symmetry of their coordination polyhedra can be described as a distorted square antiprism.

The UV−vis absorption properties of **L** have been determined in CH_2Cl_2 solution and rationalized by TD-DFT calculations. All of the lowest-energy absorption bands have been attributed to ILCT bands, while the higher energy bands have been, respectively, attributed to ID and IA transitions.

Upon irradiation of the HOMO → LUMO-type intraligand charge transfer the $^2F_{5/2} \rightarrow {}^2F_{7/2}$ ytterbium-centered luminescence was sensitized through an efficient antenna effect of the organic chromophore **L**.

For **1** and **3**, the thermal dependence of the magnetic susceptibilities has been reproduced and/or fitted using both Stevens operators and ab initio methods in order to extract quantitative values of the crystal field splitting. Interestingly, single-molecule magnet behavior is observed for the dysprosium derivatives with better dynamic characteristics for **3** than for **1**. On the basis of the results of ab initio calculations, this observation has been attributed to the increase of symmetry and electronic charge redistribution of **3** compared to **1**, while the size of the π system of the nitrogenated ligand has no significant effect on the magnetic properties. A parallel between the energy splitting value determined from the luminescence and magnetic properties has been realized.

In future work, the presence of the redox-active TTF core opens the way to modification of the luminescence and magnetic properties of our systems after oxidation of the TTF-based ligand.

ASSOCIATED CONTENT

Supporting Information

Crystallographic information in CIF format, crystal packing, cyclic voltammetry, first magnetization, additional details about dynamic magnetic properties, and additional ab initio calculation results. The Supporting Information is available free of charge on the ACS Publications website at DOI: 10.1021/acs.inorgchem.5b00441.

AUTHOR INFORMATION

Corresponding Authors

*E-mail: fabrice.pointillart@univ-rennes1.fr.
*E-mail: boris.leguennic@univ-rennes1.fr.
*E-mail: shi-xia.liu@dcb.unibe.ch.

Notes

The authors declare no competing financial interest.

ACKNOWLEDGMENTS

This work was supported by the CNRS, Rennes Métropole, Université de Rennes 1, Région Bretagne, FEDER, and Agence Nationale de la Recherche (No. ANR-13-BS07-0022-01) and the Swiss National Science Foundation (No. 200021-147143). B.L.G. thanks the French GENCI-CINES center for high-performance computing resources (project x2015080649).

REFERENCES

(1) (a) Bünzli, J. C. G.; Piguet, C. *Chem. Rev.* **2002**, *102*, 1897−1928. (b) Sessoli, R.; Powell, A. K. *Coord. Chem. Rev.* **2009**, *253*, 2328−2341. (c) Luzon, J.; Sessoli, R. *Dalton Trans.* **2012**, *41*, 13556−13567. (d) Tang, T.; Hewitt, I.; Madhu, N. T.; Chastanet, G.; Wernsdorfer, W.; Anson, C. E.; Benelli, C.; Sessoli, R.; Powell, A. K. *Angew. Chem., Int. Ed.* **2006**, *45*, 1729−1733.

(2) (a) Car, P. E.; Perfetti, M.; Mannini, M.; Favre, A.; Caneschi, A.; Sessoli, R. *Chem. Commun.* **2011**, *47*, 3751−3753. (b) Cucinotta, G.; Perfetti, M.; Luzon, J.; Etienne, M.; Car, P. E.; Caneschi, A.; Calvez, G.; Bernot, K.; Sessoli, R. *Angew. Chem., Int. Ed.* **2012**, *51*, 1606−1610. (c) Boulon, M.-E.; Cucinotta, G.; Luzon, J.; Degl'Innocenti, C.; Perfetti, M.; Bernot, K.; Calvez, G.; Caneschi, A.; Sessoli, R. *Angew. Chem., Int. Ed.* **2013**, *52*, 350−354.

(3) (a) Jiang, S.-D.; Wang, B.-W.; Su, G.; Wang, Z.-M.; Gao, S. *Angew. Chem., Int. Ed.* **2010**, *49*, 7448−7451. (b) Layfield, R. A.; Mcdouall, J. J. W.; Sulway, S. A.; Tuna, F.; Collison, D.; Winpenny, R. E. P. *Chem.—Eur. J.* **2010**, *16*, 4442−4446. (c) Jiang, S.-D.; Liu, S.-S.; Zhou, L.-N.; Wang, B.-W.; Wang, Z.-M.; Gao, S. *Inorg. Chem.* **2012**, *51*, 3079−3087. (d) Jiang, S.-D.; Wang, B.-W.; Sun, H.-L.; Wang, Z.-M.; Gao, S. *J. Am. Chem. Soc.* **2011**, *133*, 4730−4733. (e) Jeletic, M.; Lin, P.-H.; Le Roy, J. J.; Korobkov, I.; Gorelsky, S. I.; Murugesu, M. *J. Am. Chem. Soc.* **2011**, *133*, 19286−19289. (f) Ungur, L.; Le Roy, J. J.; Korobkov, I.; Murugesu, M.; Chibotaru, L. F. *Angew. Chem., Int. Ed.* **2014**, *53*, 4413−4417. (g) Meihaus, K. R.; Long, J. R. *J. Am. Chem. Soc.* **2013**, *135*, 17952−17957. (h) Le Roy, J. J.; Korobkov, I.; Murugesu, M. *Chem. Commun.* **2014**, *50*, 1602−1604.

(4) Ishikawa, N.; Sugita, M.; Ishikawa, T.; Koshihara, S.; Kaizu, Y. *J. Am. Chem. Soc.* **2003**, *125*, 8694−8695.

(5) (a) Rinehart, J. D.; Long, J. R. *Chem. Sci.* **2011**, *2*, 2078−2085. (b) Baldovi, J. J.; Cardona-Serra, S.; Clemente-Juan, J. M.; Coronado, E.; Gaita-Arino, A.; Palii, A. *Inorg. Chem.* **2012**, *51*, 12565−12574. (c) Aravena, D.; Ruiz, E. *Inorg. Chem.* **2013**, *52*, 13770−13778. (d) Chilton, N. F.; Collison, D.; McInnes, E. J. L.; Winpenny, R. E. P.; Soncini, A. *Nat. Commun.* **2013**, *5*, 673−678.

DOI: 10.1021/acs.inorgchem.5b00441
Inorg. Chem. 2015, 54, 5384−5397

(6) (a) Bünzli, J.-C. G. *Acc. Chem. Res.* **2006**, *39*, 53−61. (b) Eliseeva, S. V.; Bünzli, J.-C. G. *Chem. Soc. Rev.* **2010**, *39*, 189−227. (c) Eliseeva, S. V.; Bünzli, J.-C. G. In *Lanthanide spectroscopy, Materials, and Bio-applications*; Hänninen, P., Härmä, H., Eds.; Springer Series on Fluorescence; Springer Verlag: Berlin, 2010; Vol. 7, Chapter 1. (d) In *Luminescence of Lanthanide Ions in Coordination Compounds and Nanomaterials*; De Bettencourt-Diaz, A., Eds.; Wiley: New York, 2014.

(7) (a) Faulkner, S.; Pope, S. J. A.; Burton-Pye, B. P. *Appl. Spectrosc. Rev.* **2005**, *40*, 1−31. (b) Gunnlaugsson, T.; Stomeo, F. *Org. Biomol. Chem.* **2007**, *5*, 1999−2009. (c) Montgomery, C. P.; Murray, B. S.; New, E. J.; Pal, R.; Parker, D. *Acc. Chem. Res.* **2009**, *42*, 925−937. (d) Moore, E. G.; Samuel, A. P. S.; Raymond, K. N. *Acc. Chem. Res.* **2009**, *42*, 542−552. (e) D'Aléo, A.; Bourdolle, A.; Bulstein, S.; Fauquier, T.; Grichine, A.; Duperray, A.; Baldeck, P. L.; Andraud, C.; Brasselet, S.; Maury, O. *Angew. Chem. In. Ed.* **2012**, *51*, 6622−6625.

(8) (a) Polman, A.; van Veggel, F. C. J. M. *J. Opt. Soc. Am. B* **2004**, *21*, 871−892. (b) Banerjee, S.; Huebner, L.; Romanelli, M. D.; Kumar, G. A.; Riman, R. E.; Emge, T. J.; Brennan, J. G. *J. Am. Chem. Soc.* **2005**, *127*, 15900−15906. (c) Riman, R. E.; Kumar, G. A.; Banerjee, S.; Brennan, J. G. *J. Am. Ceram. Soc.* **2006**, *89*, 1809−1815. (d) Kumar, G. A.; Riman, R. E.; Diaz Torres, L. A.; Banerjee, S.; Romanelli, M. D.; Emge, T. J.; Brennan, J. G. *Chem. Mater.* **2007**, *19*, 2937−2946. (e) Banerjee, S.; Kumar, G. A.; Riman, R. E.; Emge, T. J.; Brennan, J. G. *J. Am. Chem. Soc.* **2007**, *129*, 5926−5931. (f) Romanelli, M.; Kumar, G. A.; Emge, T. J.; Riman, R. E.; Brennan, J. G. *Angew. Chem., Int. Ed.* **2008**, *47*, 6049−6051. (g) Song, L.; Liu, X.; Zhen, Z.; Chen, C.; Zhang, D. J. *Mater. Chem.* **2007**, *17*, 4586−4590.

(9) (a) Bünzli, J.-C. G.; Eliseeva, S. V. *J. Rare Earths* **2010**, *28*, 824−842. (b) Kido, J.; Okamoto, Y. *Chem. Rev.* **2002**, *102*, 2347−2356. (c) McGehee, M. D.; Bergstedt, T.; Zhang, C.; Saab, A. P.; O'Regan, M. B.; Bazan, G. C.; Srdanov, V. I.; Heeger, A. J. *Adv. Mater.* **1999**, *11*, 1349−1354. (d) de Bettencourt-Dias, A. *Dalton Trans.* **2007**, 2229−2241.

(10) (a) Long, J.; Vallat, R.; Ferreira, R. A. S.; Carlos, L. D.; Paz, F. A. A.; Guari, Y.; Larionova, J. *Chem. Commun.* **2012**, *48*, 9974−9976. (b) Yamashita, K.; Miyazaki, R.; Kataoka, Y.; Nakanishi, T.; Hasegawa, Y.; Nakano, M.; Yamamura, T.; Kajiwara, T. *Dalton Trans.* **2013**, *42*, 1987−1990. (c) Ehama, K.; Ohmichi, Y.; Sakamoto, S.; Fujinami, T.; Matsumoto, N.; Mochida, N.; Ishida, T.; Sunatsuki, Y.; Tsuchimoto, M.; Re, N. *Inorg. Chem.* **2013**, *52*, 12828−12841. (d) Pointillart, F.; Le Guennic, B.; Golhen, S.; Cador, O.; Maury, O.; Ouahab, L. *Chem. Commun.* **2013**, *49*, 615−617. (e) Pointillart, F.; Le Guennic, B.; Cauchy, T.; Golhen, S.; Cador, O.; Maury, O.; Ouahab, L. *Inorg. Chem.* **2013**, *52*, 5978−5990. (f) Cosquer, G.; Pointillart, F.; Jung, J.; Le Guennic, B.; Golhen, S.; Cador, O.; Guyot, Y.; Brenier, A.; Maury, O.; Ouahab, L. *Eur. J. Inorg. Chem.* **2014**, 69−82.

(11) (a) Tanaka, H.; Kobayashi, H.; Kobayashi, A.; Cassoux, P. *Adv. Mater.* **2000**, *12*, 1685−1689. (b) Uji, S.; Shinagawa, H.; Terashima, T.; Terakura, C.; Yakabe, T.; Terai, Y.; Tokumoto, M.; Kobayashi, A.; Tanaka, H.; Kobayashi, H. *Nature* **2001**, *410*, 908−910. (c) Kobayashi, A.; Fujiwara, E.; Kobayashi, H. *Chem. Rev.* **2004**, *104*, 5243−5264. (d) Enoki, T.; Miyasaki, A. *Chem. Rev.* **2004**, *104*, 5449−5478. (e) Coronado, E.; Day, P. *Chem. Rev.* **2004**, *104*, 5419−5448. (f) Ouahab, L.; Enoki, T. *Eur. J. Inorg. Chem.* **2004**, 933−941. (g) Fujiwara, H.; Wada, K.; Hiraoka, T.; Hayashi, T.; Sugimoto, T.; Nakazumi, H.; Yokogawa, K.; Teramura, M.; Yasuzuka, S.; Murata, K.; Mori, T. *J. Am. Chem. Soc.* **2005**, *127*, 14166−14167. (h) Kato, R. *Bull. Chem. Soc. Jpn.* **2000**, *73*, 515−534. (i) Lorcy, D.; Bellec, N.; Fourmigué, M.; Avarvari, N. *Coord. Chem. Rev.* **2009**, *253*, 1398−1438. and references therein. (j) Pointillart, F.; Golhen, S.; Cador, O.; Ouahab, L. *Dalton Trans.* **2013**, *42*, 1949−1960 and references therein..

(12) (a) Faulkner, S.; Burton-Pye, B. P.; Khan, T.; Martin, L. R.; Wray, S. D.; Skabara, P. J. *Chem. Commun.* **2002**, *16*, 1668−1669. (b) Pope, S. J. A.; Burton-Pye, B. P.; Berridge, R.; Khan, T.; Skabara, P.; Faulkner, S. *Dalton Trans.* **2006**, 2907−2912. (c) Pointillart, F.; Cauchy, T.; Maury, O.; Le Gal, Y.; Golhen, S.; Cador, O.; Ouahab, L. *Chem.—Eur. J.* **2010**, *16*, 11926−11941. (d) Pointillart, F.; Bourdolle, A.; Cauchy, T.; Maury, O.; Le Gal, Y.; Golhen, S.; Cador, O.; Ouahab, L. *Inorg. Chem.* **2012**, *51*, 978−984. (e) D'Aléo, A.; Pointillart, F.; Ouahab, L.; Andraud, C.; Maury, O. *Coord. Chem. Rev.* **2012**, *256*, 1604−1620. (f) Pointillart, F.; Le Guennic, B.; Golhen, S.; Cador, O.; Maury, O.; Ouahab, L. *Inorg. Chem.* **2013**, *52*, 1610−1620. (g) Feng, M.; Pointillart, F.; Le Guennic, B.; Lefeuvre, B.; Golhen, S.; Cador, O.; Maury, O.; Ouahab, L. *Chem. Asian. J.* **2014**, *9*, 2814−2825.

(13) (a) Pointillart, F.; Le Gal, Y.; Golhen, S.; Cador, O.; Ouahab, L. *Chem.—Eur. J.* **2011**, *17*, 10397−10404. (b) Pointillart, F.; Klementieva, S.; Kuropatov, V.; Le Gal, Y.; Golhen, S.; Cador, O.; Cherkasov, V.; Ouahab, L. *Chem. Commun.* **2012**, *48*, 714−716. (c) Pointillart, F.; Le Guennic, B.; Cauchy, T.; Golhen, S.; Cador, O.; Maury, O.; Ouahab, L. *Inorg. Chem.* **2013**, *52*, 5978−5990. (d) Gao, F.; Cui, L.; Liu, W.; Hu, L.; Zhong, Y.-W.; Li, Y.-Z.; Zuo, J.-L. *Inorg. Chem.* **2013**, *52*, 11164−11172. (e) da Cunha, T. T.; Jung, J.; Boulon, M.-E.; Campo, G.; Pointillart, F.; Pereira, C. L. M.; Le Guennic, B.; Cador, O.; Bernot, K.; Pineider, F.; Golhen, S.; Ouahab, L. *J. Am. Chem. Soc.* **2013**, *135*, 16332−16335. (f) Pointillart, F.; Golhen, S.; Cador, O.; Ouahab, L. *Eur. J. Inorg. Chem.* **2014**, 4558−4563. (g) Jung, J.; Cador, O.; Bernot, K.; Pointillart, F.; Luzon, J.; Le Guennic, B. *Beilstein J. Nanotechnol.* **2014**, *5*, 2267−2274. (h) Pointillart, F.; Bernot, K.; Le Guennic, B.; Golhen, S.; Cador, O.; Ouahab, L. *Angew. Chem., Int. Ed.* **2015**, *54*, 1504−1507.

(14) (a) Jia, C.; Liu, S.-X.; Tanner, C.; Leiggener, C.; Neels, A.; Sanguinet, L.; Levillain, E.; Leutwyler, S.; Hauser, A.; Decurtins, S. *Chem.—Eur. J.* **2007**, *13*, 3804−3812. (b) Goze, C.; Leiggener, C.; Liu, S.-X.; Sanguinet, L.; Levillain, E.; Hauser, A.; Decurtins, S. *ChemPhysChem* **2007**, *8*, 1504−1512. (c) Ran, Y.-F.; Steinmann, M.; Sigrist, M.; Liu, S.-X.; Hauser, J.; Decurtins, S. *C. R. Chimie* **2012**, *15*, 838−844. (d) Dupont, N.; Ran, Y.-F.; Liu, S.-X.; Grilj, J.; Vauthey, E.; Decurtins, S.; Hauser, A. *Inorg. Chem.* **2013**, *52*, 306−312. (e) Lapadula, G.; Trummer, D.; Conley, M. P.; Steinmann, M.; Ran, Y.-F.; Brasselet, S.; Guyot, Y.; Maury, O.; Decurtins, S.; Liu, S.-X.; Copéret, C. *Chem. Mater.* **2015**, *27*, 2033−2037.

(15) (a) Wang, Y.; Li, X. L.; Wang, T. W.; Song, Y.; You, X. Z. *Inorg. Chem.* **2010**, *49*, 969−976. (b) Li, D.-P.; Wang, T.-W.; Li, C.-H.; Liu, D.-S.; Li, Y.-Z.; You, X.-Z. *Chem. Commun.* **2010**, *46*, 2929−2931. (c) Norel, L.; Bernot, K.; Feng, M.; Roisnel, T.; Caneschi, A.; Sessoli, R.; Rigaut, S. *Chem. Commun.* **2012**, *48*, 3948−3950.

(16) (a) Richardson, M. F.; Wagner, W. F.; Sands, D. E. *J. Inorg. Nucl. Chem.* **1968**, *30*, 1275−1289. (b) Vooshin, A. I.; Shavaleev, N. M.; Kazakov, V. P. *J. Lumin.* **2000**, *91*, 49−58.

(17) (a) Sheldrick, G. M. *SHELX97, Programs for Crystal Structure Analysis (Release 97-2)*; Institut für Anorganische Chemie der Universität: Göttingen, Germany, 1998. (b) SIR97: Altomare, A.; Burla, M. C.; Camalli, M.; Cascarano, G. L.; Giacovazzo, C.; Guagliardi, A.; Moliterni, A. G. G.; Polidori, G.; Spagna, R. *J. Appl. Crystallogr.* **1999**, *32*, 115−119.

(18) Frisch, M. J.; Trucks, G. W.; Schlegel, H. B.; Scuseria, G. E.; Robb, M. A.; Cheeseman, J. R.; Scalmani, G.; Barone, V.; Mennucci, B.; Petersson, G. A.; Nakatsuji, H.; Caricato, M.; Li, X.; Hratchian, H. P.; Izmaylov, A. F.; Bloino, J.; Zheng, G.; Sonnenberg, J. L.; Hada, M.; Ehara, M.; Toyota, K.; Fukuda, R.; Hasegawa, J.; Ishida, M.; Nakajima, T.; Honda, Y.; Kitao, O.; Nakai, H.; Vreven, T.; Montgomery, Jr. J. A.; Peralta, J. E.; Ogliaro, F.; Bearpark, M.; Heyd, J. J.; Brothers, E.; Kudin, K. N.; Staroverov, V. N.; Kobayashi, R.; Normand, J.; Raghavachari, K.; Rendell, A.; Burant, J. C.; Iyengar, S. S.; Tomasi, J.; Cossi, M.; Rega, N.; Millam, J. M.; Klene, M.; Knox, J. E.; Cross, J. B.; Bakken, V.; Adamo, C.; Jaramillo, J.; Gomperts, R.; Stratmann, R. E.; Yazyev, O.; Austin, A. J.; Cammi, R.; Pomelli, C.; Ochterski, J. W.; Martin, R. L.; Morokuma, K.; Zakrzewski, V. G.; Voth, G. A.; Salvador, P.; Dannenberg, J. J.; Dapprich, S.; Daniels, A. D.; Farkas, O.; Foresman, J. B.; Ortiz, J. V.; Cioslowski, J.; Fox, D. J. *Gaussian 09*, Revision A.02; Gaussian Inc.: Wallingford, CT, 2009.

(19) (a) Perdew, J. P.; Burke, K.; Ernzerhof, M. *Phys. Rev. Lett.* **1996**, *77*, 3865−3868. (b) Adamo, C.; Barone, V. *J. Chem. Phys.* **1999**, *110*, 6158−6170.

(20) Dolg, M.; Stoll, H.; Preuss, H. *Theor. Chim. Acta* **1993**, *85*, 441−450.

DOI: 10.1021/acs.inorgchem.5b00441
Inorg. Chem. 2015, 54, 5384−5397

(21) Weigend, F.; Ahlrichs, R. *Phys. Chem. Chem. Phys.* **2005**, *7*, 3297−3305.
(22) Tomasi, J.; Mennucci, B.; Cammi, R. *Chem. Rev.* **2005**, *105*, 2999−3093.
(23) (a) Cossi, M.; Barone, V. *J. Chem. Phys.* **2001**, *115*, 4708−4717. (b) Improta, R.; Barone, V.; Scalmani, G.; Frisch, M. J. *J. Chem. Phys.* **2006**, *125*, 054103−054109.
(24) Allouche, A.-R. *J. Comput. Chem.* **2011**, *32*, 174−182.
(25) Aquilante, F.; De Vico, L.; Ferré, N.; Ghigo, G.; Malmqvist, P.-A.; Neograd y, P.; Bondo Pedersen, T.; Pitonak, M.; Reiher, M.; Roos, B. O.; Serrano-Andrés, L.; Urban, M.; Veryazov, V.; Lindh, R. *J. Comput. Chem.* **2010**, *31*, 224−247.
(26) Roos, B. O.; Taylor, P. R.; Siegbahn, P. E. M. *Chem. Phys.* **1980**, *48*, 157−288.
(27) (a) Malmqvist, P. A.; Roos, B. O.; Schimmelpfennig, B. *Chem. Phys. Lett.* **2002**, *357*, 230−240. (b) Malmqvist, P.- Å.; Roos, B. O. *Chem. Phys. Lett.* **1989**, *155*, 189−194.
(28) (a) Chibotaru, L. F.; Ungur, L. *J. Chem. Phys.* **2012**, *137*, 064112−064122. (b) Chibotaru, L.; Ungur, L.; Soncini, A. *Angew. Chem., Int. Ed.* **2008**, *47*, 4126−4129.
(29) Aquilante, F.; Malmqvist, P.-Å.; Pedersen, T. B.; Ghosh, A.; Roos, B. O. *J. Chem. Theory Comput.* **2008**, *4*, 694−702.
(30) (a) Roos, B. O.; Lindh, R.; Malmqvist, P.-A.; Veryazov, V.; Widmark, P.-O. *J. Phys. Chem. A* **2004**, *108*, 2851−2858. (b) Roos, B. O.; Lindh, R.; Malmqvist, P.-A.; Veryazov, V.; Widmark, P.-O. *J. Phys. Chem. A* **2005**, *109*, 6576−6586. (c) Roos, B. O.; Lindh, R.; Malmqvist, P.-Å.; Veryazov, V.; Widmark, P.-O.; Borin, A. C. *J. Phys. Chem. A* **2008**, *112*, 11431−11435.
(31) Llunell, M.; Casanova, D.; Cirera, J.; Bofill, J. M.; Alemany, P.; Alvarez, S. *SHAPE* (version 2.1); Barcelona, 2013.
(32) (a) Lorcy, D.; Bellec, N.; Fourmigué, M.; Avarvari, N. *Coord. Chem. Rev.* **2009**, *253*, 1398−1438 and references therein. (b) Pointillart, F.; Golhen, S.; Cador, O.; Ouahab, L. *Dalton Trans.* **2013**, *42*, 1949−1960.
(33) Kahn, O. *Molecular Magnetism*; VCH: Weinhem, 1993.
(34) (a) Orbach, R. *Proc. Phys. Soc. A* **1961**, *264*, 458−484. (b) Rudowicz, C. *J. Phys. C: Solid State Phys.* **1985**, *18*, 1415−1430.
(35) Görlder-Walrand, C.; Binnemans, K. *Handb. Phys. Chem. Rare Earths* **1996**, *23*, 121.
(36) Cosquer, G.; Pointillart, F.; Golhen, S.; Cador, O.; Ouahab, L. *Chem.—Eur. J.* **2013**, *19*, 7895−7903.
(37) Chen, G.-J.; Guo, Y.-N.; Tian, J.-L.; Tang, J.; Gu, W.; Liu, X.; Yan, S.-P.; Cheng, P.; Liao, D.-Z. *Chem.—Eur. J.* **2012**, *18*, 2484−2487.
(38) (a) Cosquer, G.; Pointillart, F.; Jung, J.; Le Guennic, B.; Golhen, S.; Cador, O.; Guyot, Y.; Brenier, A.; Maury, O.; Ouahab, L. *Eur. J. Inorg. Chem.* **2014**, 69−82. (b) Jung, J.; T. da Cunha, T.; Le Guennic, B.; Pointillart, F.; L. M. Pereira, C.; Luzon, J.; Golhen, S.; Cador, O.; Maury, O.; Ouahab, L. *Eur. J. Inorg. Chem.* **2014**, 3888−3894.
(39) (a) Liu, J.-L.; Yuan, K.; Leng, J.-D.; Ungur, L.; Wernsdorfer, W.; Guo, F.-S.; Chibotaru, L. F.; Tong, M.-L. *Inorg. Chem.* **2012**, *51*, 8538−8544. (b) Lin, P.-H.; Sun, W.-S.; Tian, Y.-M.; Yan, P.-F.; Ungur, L.; Chibotaru, L. F.; Murugesu, M. *Dalton Trans.* **2012**, *41*, 12349−12352. (c) Bandeira, N. A. G.; Daniel, C.; Trifonov, A.; Calhorda, M. J. *Organometallics* **2012**, *31*, 4693−4700.
(40) Cosquer, G.; Pointillart, F.; Le Guennic, B.; Le Gal, Y.; Golhen, S.; Cador, O.; Ouahab, L. *Inorg. Chem.* **2012**, *51*, 8488−8501.
(41) Bourdolle; Allali, M.; D'Aléo, A.; Baldeck, P. L.; Kamada, K.; Williams, J. A. G.; Le Bozec, H.; Andraud, C.; Maury, O. *ChemPhysChem* **2013**, *14*, 3361−3367.
(42) Gonçalves Silva, F. R.; Malta, O. L.; Reinhard, C.; Güdel, H. U.; Piguet, C.; Moser, J.; Bünzli, J.-C. G. *J. Phys. Chem. A* **2002**, *106*, 1670−1677.

DOI: 10.1021/acs.inorgchem.5b00441
Inorg. Chem. 2015, 54, 5384−5397